Chemical Science

EDGE ARTICLE

View Article Online
View Journal | View Issue



Cite this: *Chem. Sci.*, 2018, **9**, 2179

# Injectable hyperbranched poly(β-amino ester) hydrogels with on-demand degradation profiles to match wound healing processes†

Qian Xu,[a] Linru Guo,[b] Sigen A,[a] Yongsheng Gao,[a] Dezhong Zhou,[a] Udo Greiser,[a] Jack Creagh-Flynn,[a] Hong Zhang,[a] Yixiao Dong,[a] Lara Cutlar,[a] Fagang Wang,[c] Wenguang Liu,[b] Wei Wang*[ab] and Wenxin Wang*[ab]

Adjusting biomaterial degradation profiles to match tissue regeneration is a challenging issue. Herein, biodegradable hyperbranched poly(β-amino ester)s (HP-PBAEs) were designed and synthesized *via* "A2 + B4" Michael addition polymerization, and displayed fast gelation with thiolated hyaluronic acid (HA-SH) *via* a "click" thiol–ene reaction. HP-PBAE/HA-SH hydrogels showed tunable degradation profiles both *in vitro* and *in vivo* using diamines with different alkyl chain lengths and poly(ethylene glycol) diacrylates with varied PEG spacers. The hydrogels with optimized degradation profiles encapsulating ADSCs were used as injectable hydrogels to treat two different types of humanized excisional wounds – acute wounds with faster healing rates and diabetic wounds with slower healing and neo-tissue formation. The fast-degrading hydrogel showed accelerated wound closure in acute wounds, while the slow-degrading hydrogel showed better wound healing for diabetic wounds. The results demonstrate that the new HP-PBAE-based hydrogel in combination with ADSCs can be used as a well-controlled biodegradable skin substitute, which demonstrates a promising approach in the treatment of various types of skin wounds.

Received 6th September 2017
Accepted 4th January 2018

DOI: 10.1039/c7sc03913a

rsc.li/chemical-science



## Introduction

One focal issue for the optimization of biomaterials for tissue regeneration has been the tuning of degradation rates to match the wound healing process. A rapid degradation rate cannot impart the hydrogels with sufficient support for neo-tissue ingrowth. On the other hand, too slow a degradation rate will cause disturbed tissue development.[1–3] In addition, it is important that the degradation can control the release of therapeutic cells or exogenous factors.[4] Injectable hydrogels, with the ability to be introduced through minimal invasion and to fill any defect or cavity, have been extensively used for cell delivery in tissue regeneration in recent years.[5–7] However, due to limited control of the material degradation process to match tissue integration, so far the developed injectable hydrogels have not fulfilled their potential.[1]

The unique pathophysiological abnormalities in different wound sites require a diversity of degradation rates of the biomaterials for functional tissue regeneration. An acute wound without disturbance in the healing process may achieve quick healing. As for chronic wounds, such as diabetic wounds (a severe complication of diabetes and frequently leading to amputation or death[8]), the pathogenic abnormalities in the wound site slow down the healing process.[9] In this regard, by tuning the material degradation rates to match the rates of tissue formation, both normal physiological wounds and chronic wounds can proceed through orderly and timely reparation.

Poly(β-amino ester)s (PBAEs), synthesized *via* Michael addition between amines and acrylates, have attracted broad attention in recent years due to their highly flexible chemical compositions and properties, ease of synthesis, and low cost.[10–12] The multiple ester groups on the backbone result in the degradation of PBAEs by hydrolysis in physiological conditions with non-cytotoxic amino acids and diols as side products. Due to these advantages, PBAEs have been widely utilized in biomedical applications. Langer and Anderson *et al.* have synthesized more than 2500 linear poly(β-amino ester)s (LPBAEs) as non-viral gene vectors which showed high gene transfection efficiency[10,13,14] and excellent biosafety in animal experiments (*e.g.* rodents).[15–17] Moreover, LPBAEs were also demonstrated as photo-crosslinkable macromers for the preparation of biodegradable crosslinked materials.[18–20] However, significant limitations relating to the linear structure of LPBAE macromers render them less optimal candidates for hydrogel

[a]*Charles Institute of Dermatology, School of Medicine, University College Dublin, Dublin 4, Ireland. E-mail: wwgfz@tju.edu.cn; wenxin.wang@ucd.ie*

[b]*School of Materials Science and Engineering, Tianjin Key Laboratory of Composite and Functional Materials, Tianjin University, Tianjin 300350, China*

[c]*Department of Burn & Plastic Surgery, Shandong Provincial Hospital Affiliated to Shandong University, Jinan 250001, China*

† Electronic supplementary information (ESI) available. See DOI: 10.1039/c7sc03913a

formation. Firstly, these LPBAE macromers with only two end acrylate functional groups result in materials with less crosslinking and weak mechanical strength. Secondly, to acquire LPBAE macromers terminated with acrylate groups, only low molecular weight oligomers (<6 kDa) can be synthesized because an excessive feed ratio of diacrylate to amine is needed. Due to the nature of the step-wise polymerization reaction, an increase in the feed ratio of diacrylate to amine has a substantial effect on yielding LPBAE macromers with low molecular weights (2–4 kDa).[19] For instance, Anderson *et al.* synthesized a library of LPBAE macromers with a diacrylate to amine ratio of 1.2 : 1 only resulting in molecular weights of approximately 4 kDa.[20] Thirdly, the amount of terminal vinyl groups is further reduced by the increase of molecular weight, resulting in a slow gelation rate and low gel fraction in the LPBAE macromer gelation system. It is a significant concern for the application of LPBAEs in biomedical fields that the gel fraction for LPBAE macromers (5–6 kDa) was only approximately 50%, suggesting that a high number of the polymer chains were not involved in the crosslinked network and would be released upon swelling of the network.[18] Finally, the poor water solubility makes it very difficult for LPBAE macromers to form hydrogel systems and therefore compromises the practical application. Hyperbranched polymers are highly branched macromolecules with three-dimensional dendritic architectures. Their globular and dendritic architectures demonstrate unique properties such as abundant functional groups and good solubility. Thus, hyperbranched polymers with abundant terminal groups have shown more promise as injectable hydrogels.[18,21,22] We hypothesize that PBAEs with hyperbranched structures can address the aforementioned obstacles and facilitate the fabrication of PBAE injectable hydrogel systems with diverse and tunable degradation rates.

In this paper, we have demonstrated the synthesis of a series of hyperbranched PBAEs (HP-PBAEs) *via* "A2 + B4" Michael addition methodology[23] – an approach traditionally considered to directly form crosslinked structures with poor control (Fig. 1). HP-PBAEs display a fast gelation process with thiolated hyaluronic acid (HA-SH) *via* a "click" thiol–ene reaction leading to the formation of HP-PBAE hydrogels with controllable and adjustable degradation profiles. Two hydrogels with optimized degradation rates were used to encapsulate ADSCs and further injected onto humanized excisional wounds (the humanized wound model can better mimic the human cutaneous healing process[24,25]). Hydrogels with a faster degradation rate exhibited better wound healing in nondiabetic wounds, while hydrogels with a slower degradation rate showed a faster wound closure rate and significantly promoted the healing process as evidenced by histological assays for diabetic wounds.

# Results

### Synthesis and characterization of HP-PBAEs

The "A2 + B4" Michael addition polymerization approach developed for the design and synthesis of HP-PBAEs (Fig. 1A) was traditionally considered as a typical crosslinking reaction leading to the bulky crosslinked structure of a gel. However, we have demonstrated that through control of the reaction kinetics, the diacrylate (A2) to diamine (B4) reaction can be well controlled. Moreover, the feed ratio of A2 to B4 needs to be considered carefully in order to generate hyperbranched polymers with the targeted molecular weight and required terminal groups. The results showed that a high feed ratio of diacrylate (A2) to diamine (B4) (*e.g.*, 3 : 1) only produced HP-PBAEs with a low molecular weight (2–5 kDa) while a low feed ratio (*e.g.*, 2.2 : 1) led to fast gelation. Therefore, a feed ratio of 2.5 : 1 was selected with the aim of generating acrylate-terminated HP-PBAEs with a molecular weight of approximately 10 kDa. By varying the monomer combination of PEGDA (258, 575, and 700 Da) and diamine (ethylenediamine (EDA) and hexamethylenediamine (HDA)), a total of six HP-PBAEs were synthesized (ESI Table 1†). The resulting HP-PBAEs are named by the molecular weight of PEGDA and the type of diamine. For example, 700-EDA stands for HP-PBAE synthesized from PEGDA (700 Da) and EDA. The gel permeation chromatography (GPC) results are shown in ESI Fig. S1–S3,† and indicate a controlled polymerization without the occurrence of spontaneous gelation. The Mark–Houwink $\alpha$ values of the synthesised HP-PBAEs were all between 0.32 and 0.38 (ESI Fig. S4†). Since $\alpha < 0.5$ in each of these polymers, they all are shown to have a typical branched structure. The compositions of all six polymers were verified by proton nuclear magnetic resonance spectroscopy ($^1$H-NMR) (ESI Fig. S5 and S6†). The primary amine group content in the polymer backbones was also determined by picrylsulfonic acid (TNBS) assay. The results showed that there were trace amounts of amine groups left in the polymer backbone, ranging from 4.0–11.8 μmol $g^{-1}$ (ESI Fig. S7†). The well-designed hyperbranched PBAE polymers can be prepared through the "A2 + B4" strategy *via* kinetic control by stopping the reaction prior to the gelation points, which can address the limitation of the conventional "A2 + BB'B" approach.[26] The HP-PBAE polymers will hydrolytically degrade and yield small molecules in PBS buffer (ESI Fig. S8 and S9†).[20] The degradation test was monitored by GPC, and all polymers were completely degraded after 4 h (ESI Fig. S8†).

### Properties of HP-PBAE/HA-SH hydrogels

There are multiple terminal acrylate groups within HP-PBAEs providing reactive sites for rapid crosslinking to form injectable hydrogels. HA-SH, with multiple thiol groups for crosslinking *via* thiol–ene chemistry, was chosen as the crosslinker (Fig. 2A). Injectable HP-PBAE/HA-SH hydrogels were fabricated by mixing HP-PBAE solutions and HA-SH solution under mild conditions, and the resulting hydrogels were transparent and easy to handle. The gelation time at various HP-PBAE concentrations (2.5%, 5%, and 10%) was examined using the stirring method. Gelation occurs for all of the formulations in a very short time. The results revealed that higher concentrations lead to an even shorter gelation time (less than 30 seconds) and HP-PBAEs formed with a longer PEG spacer exhibit a slower gelation rate (less than 120 seconds) (Fig. 2B). Rheological measurements were further carried out to monitor the gelation rate and mechanical moduli during the gelation process (Fig. 2C and ESI S10†). Typically, the 700-EDA/HA-SH hydrogel at 10 wt% concentration exhibits a higher storage modulus (220

 

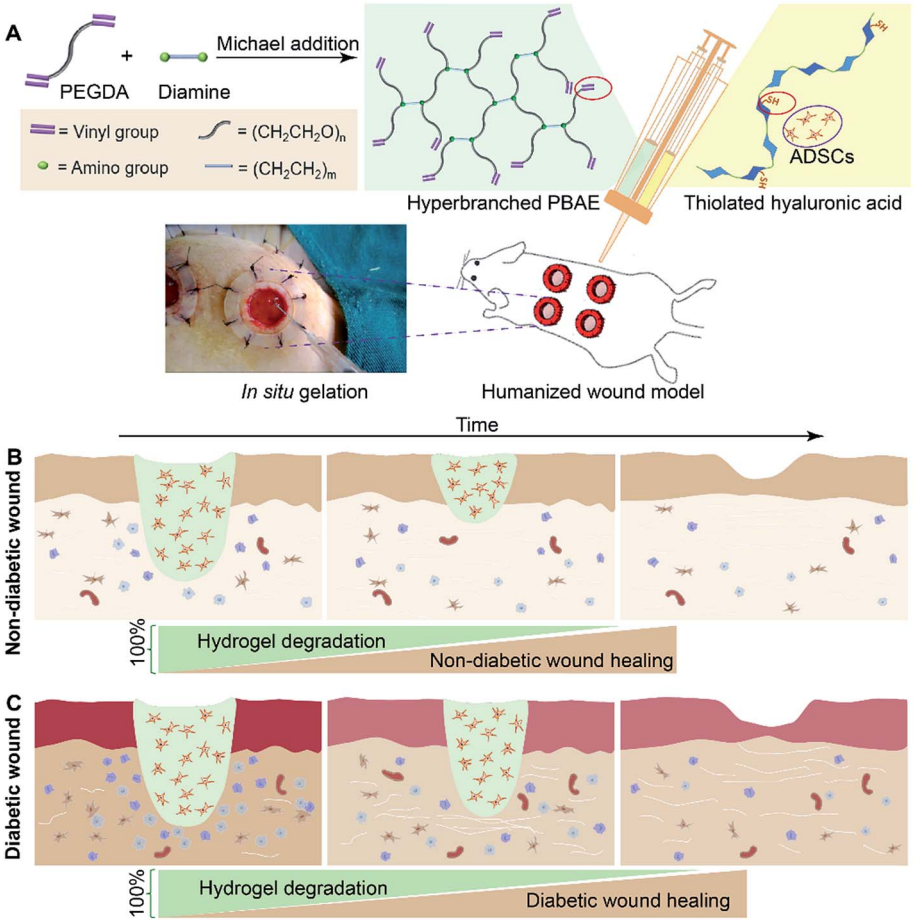


Fig. 1 A schematic of the proposed formation of HP-PBAEs and the function of HP-PBAE/HA-SH hydrogels for modulating wound healing. (A) HP-PBAEs are synthesized by the "A2 + B4" Michael addition reaction. Injectable hydrogels are formed by HP-PBAEs crosslinking with HA-SH. HP-PBAE/HA-SH/ADSCs hydrogels are mixed and injected onto full skin thickness humanized excisional wounds on the dorsum of the rats. (B) Non-diabetic wounds do not have pathophysiological abnormalities and undergo a quick healing process which correlates with the fast-degrading hydrogel. (C) Diabetic wounds possessing persistent pathophysiological defects show an impaired healing process which requires the slow-degrading hydrogel combined with therapeutic elements to optimize the healing conditions.

Pa) compared to the counterparts at 5 wt% (170 Pa) and 2.5 wt% (65 Pa) (Fig. 2D). Dynamic frequency sweep tests and strain sweep tests were also conducted, and the data are shown in ESI Fig. S11–S15.† All five hydrogels showed high strain resistance and weak frequency dependence.

### Degradation of injectable HP-PBAE/HA-SH hydrogels

To facilitate wound healing, the injectable hydrogels should not only provide mechanical support, but also be degradable at a rate which matches the regeneration of the new tissues. The degradation and water retention capacity of HP-PBAE/HA-SH hydrogels were tested in PBS at 37 °C. All of the hydrogels show similar water retention profiles (1.5 times) and retain their original shape within 12 h of incubation in PBS (Fig. 3A). 258-EDA/HA-SH hydrogels degrade completely, evidenced by the disappearance of the hydrogels at 24 h incubation. Hydrogels formed by PEGDAs (575 and 700 Da) showed relatively long degradation times. These results demonstrate the high flexibility and adjustability of HP-PBAE/HA-SH hydrogels to suit diverse yet specific application regimes.

### Biosafety and *in vivo* degradation profiles of the hydrogels

*In vitro* cytotoxicity tests of the hydrogels using the alamarBlue assay have demonstrated that HP-PBAE/HA-SH hydrogels with longer PEGDA spacers (575 and 700 Da) and shorter alkyl spacers (EDA) exhibit higher cell viability (ESI Fig. S17 and S18†).

A subcutaneous implantation was designed to assess the *in vivo* characteristics of the injectable hydrogels (5 wt%). All of the hydrogels demonstrate tunable degradation behaviors. For example, 700-EDA/HA-SH had completely degraded in 2 weeks. The weight change was 192.3% ± 9.5%, 94.6% ± 7.1% and 61.7% ± 19.4%, at days 3, 7, and 11 post-implantation, respectively (Fig. 3B). No evidence of rejection or infection was observed during the experiment, suggesting good biocompatibility of all five hydrogels. The *in vivo* degradation results showed that diamines with different alkyl intervals demonstrated a small effect on the degradation rates, while PEGDAs with varied molecular weights made a big difference. Nondiabetic and diabetic wounds without treatment demonstrate different wound closure rates (ESI Fig. S20†), and require different materials to support new tissue regeneration. Then,

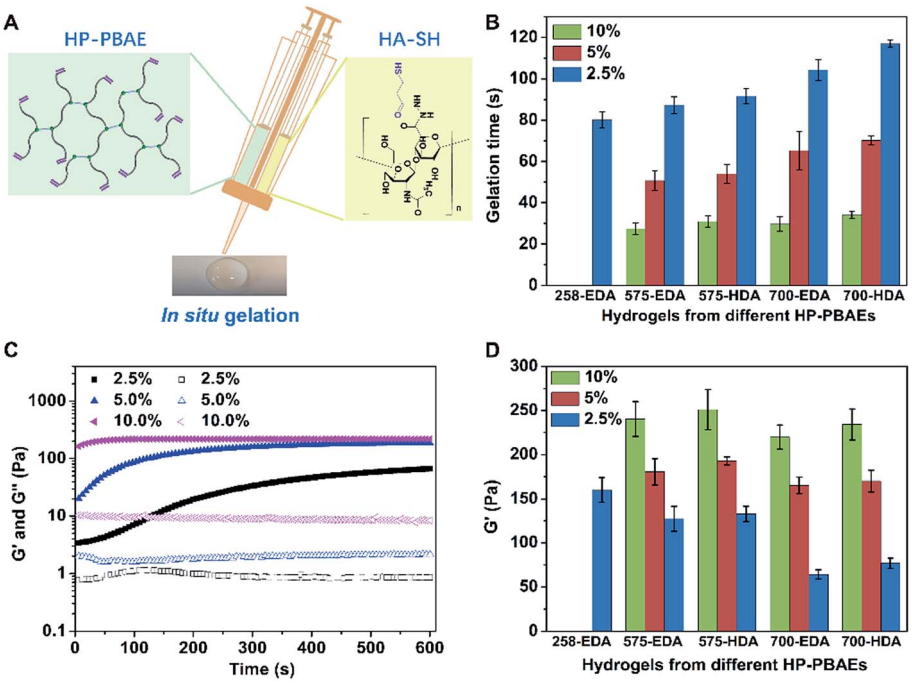


Fig. 2 The properties of injectable HP-PBAE/HA-SH hydrogels. (A) The formation of hydrogels using HA-SH to crosslink with the HP-PBAE polymer. (B) The gelation time of HP-PBAE/HA-SH hydrogels. (C) A typical gelation process of different concentrations of an injectable hydrogel (700-EDA/HA-SH) characterized by a rheometer. (D) The mechanical strength of HP-PBAE/HA-SH hydrogels.

575-EDA and 700-EDA were selected for the performance of further animal experiments in a humanized wound model (ESI Fig. S19†) due to the differences in the degradation profiles, and the degradation products of amino acids with smaller molecular weights than those of HDA polymers, which could be more rapidly metabolised *in vivo*.

### *In vivo* evaluation in nondiabetic wounds

We first investigated the effects of both hydrogels combined with ADSC therapy in a nondiabetic wound model. As shown in Fig. 4, the wound closure rate at 11 days post-wounding for both hydrogel treated wounds is significantly accelerated. The 575-EDA/HA-SH/ADSCs hydrogel treated wounds exhibit faster wound closure and thicker dermis deposition (Fig. 4C, ESI S21, and S22†). As for normal wound healing, there is no significant difference for each group in the inflammation response and re-epithelialization (Fig. 5C, G, ESI S23 and S24†). Both hydrogel treated wounds showed significantly increased vasculogenesis potential (Fig. 5D–F). The secretion of CD31, α-SMA and VEGF maintained persistently high levels even at 21 days post-wounding. However, the 575-EDA/HA-SH/ADSCs hydrogel with the faster degradation rate shows more potential for vascular tube formation than the slower one (Fig. 5D and E, $p < 0.05$).

### *In vivo* evaluation in diabetic wounds

Then, the hydrogels were investigated in humanized diabetic wound beds. At 21 days post-wounding, the PBS and ADSC treated wounds were wet with exposed granular tissue (Fig. 6A) and showed slow wound closure rates (Fig. 6B). In contrast, the hydrogel treated wounds appeared dry with intact surfaces,

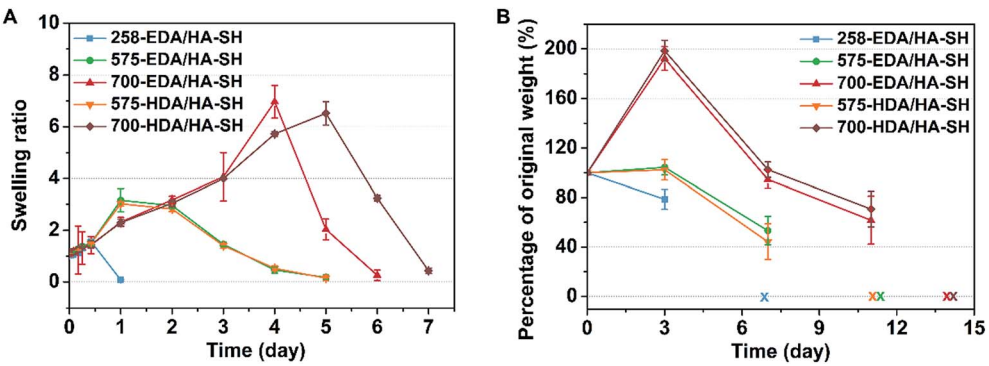


Fig. 3 The degradation profile of HP-PBAE/HA-SH hydrogels. (A) The swelling ratio of the hydrogels in PBS at 37 °C ($n = 4$). (B) The *in vivo* degradation by subcutaneous implantation. The "X" represents the time at which the hydrogels totally disappeared ($n = 4$).

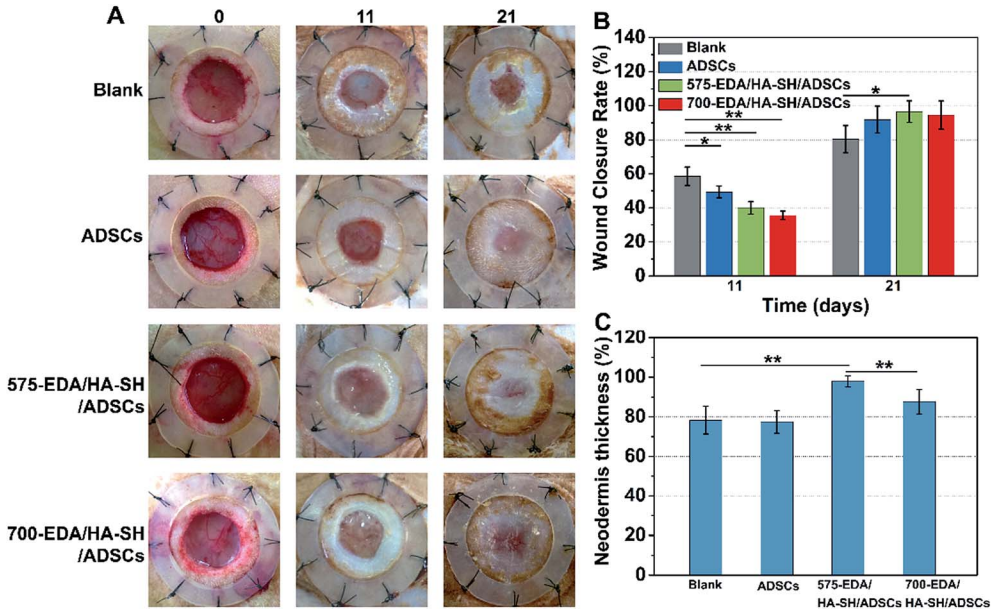


Fig. 4 Wound closure in humanized wound beds in nondiabetic rats. (A) Representative images of wound closure during 21-day *in vivo* experiments. (B) The quantification of the wound closure rate (%) over a 21-day period ($n = 8$). (C) Percentages of newly-formed tissue thickness at 21 days post-wounding. *$p < 0.05$; **$p < 0.01$.

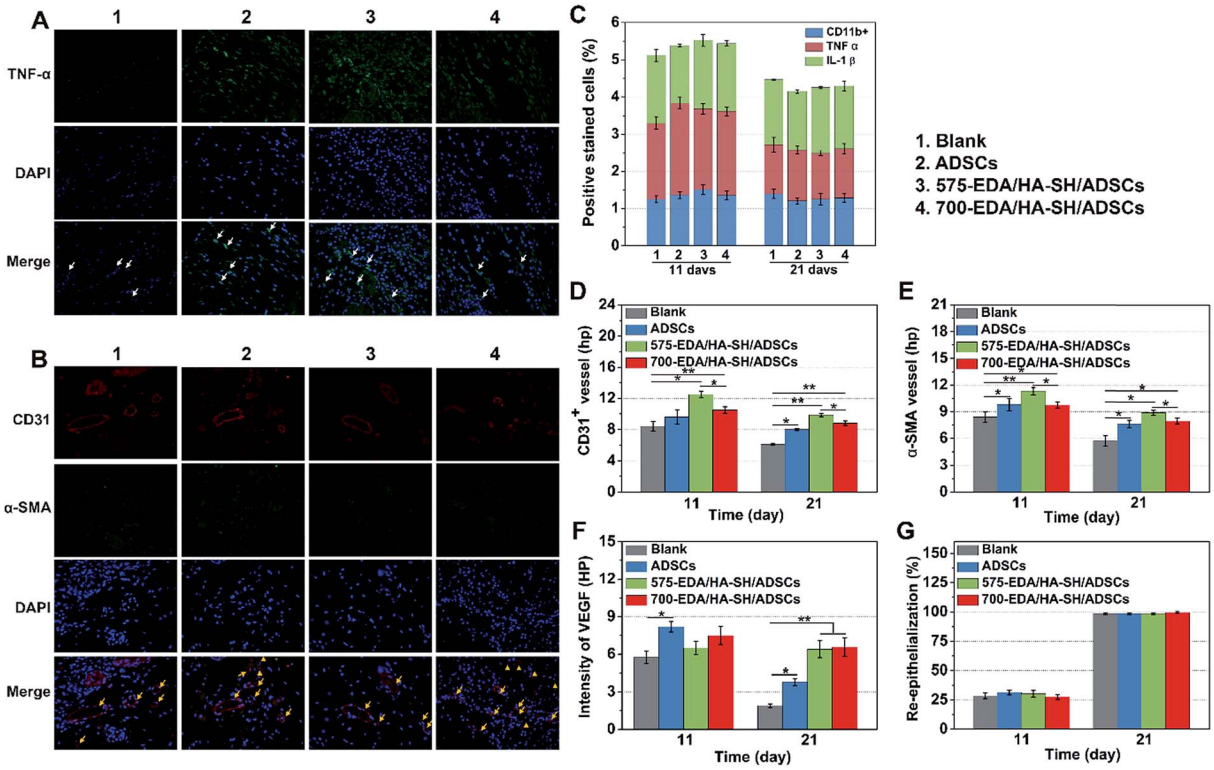


Fig. 5 The immuno-histochemical analysis of wound sections in nondiabetic wound beds at scheduled time points. (A) Representative immunofluorescent images of tissue sections at 11 days post-wounding stained for TNF-α (green) and DAPI staining for nuclei (blue). (B) CD31 (for the endothelial marker, red), α-SMA (for the endothelial myofibroblast marker, green), and DAPI (for cell nuclei, blue) stained images (21 days post-wounding). The yellow triangles represent CD31+/α-SMA− vessels, and the yellow arrows represent CD31+/α-SMA+ vessels. Scale bar: 100 μm. (C)–(G) The quantification analysis of the positive stained inflammatory cytokines, which indicates total cellular infiltration into the constructs or wound areas as well as an immune response in the surrounding tissue. (B) and (C) The quantification analysis of blood vessels based on the CD31 and α-SMA positive stained vasculature. (D) The intensity of the VEGF expression in each experimental group. (E) The quantification analysis of the re-epithelialization rate ($n = 16$ wounds per treatment group). *$p < 0.05$; **$p < 0.01$.

suggesting significantly greater wound healing. 700-EDA/HA-SH/ADSCs hydrogel treated wounds exhibited a significantly faster wound closure rate and thicker dermis reformation than the other three groups (Fig. 6B and C).

Based on the mechanisms of impaired diabetic wound healing, we performed histological and immunohistochemical analysis to understand the promoting factors for 700-EDA/HA-SH/ADSCs hydrogel treated wounds. From H&E staining, at day 11 post-wounding, all of the wounds showed a visible epidermal tongue, a substantial infiltration by nucleated cells (ESI Fig. S25†). At day 21, significantly more granulation tissue has grown and the epidermal tongue appears to be migrating towards the wound center. Masson's trichrome staining was further used to visualize collagen deposition at the wound beds (ESI Fig. S26†). Compared to the PBS counterparts, the dermis of wounds treated with 700-EDA/HA-SH/ADSCs hydrogels is much thicker (Fig. 6C, $p < 0.05$). In consistence with the dermis thickness, the collagen deposition in 700-EDA/HA-SH/ADSCs hydrogel treated wounds appears more homogenous in comparison with those treated with PBS (ESI Fig. S26†). These results correlate well with the wound repair process, which further confirms the synergistic roles of 700-EDA, HA-SH, and ADSCs in accelerating diabetic wound repair.

The inflammation, angiogenesis, and re-epithelialization responses in wound beds were further determined using immuno-histochemical and immunofluorescent staining, and the corresponding cytokine levels were quantified by Image J (Fig. 7). Long lasting inflammation is thought to be a significant reason for delayed healing. Therefore, immuno-histochemical staining for IL-1β, CD11b, and TNF-α was performed to obtain detailed understanding of the inflammation response (ESI Fig. S27†). At day 11, a substantially lower level of inflammatory factors is determined in the wounds treated with the 700-EDA/HA-SH/ADSCs hydrogel ($p < 0.05$) (Fig. 7C). Similarly, at day 21, the levels of IL-1β, TNF-α and CD11b for the PBS treated group are still much higher than for the 700-EDA/HA-SH/ADSCs treated group ($p < 0.05$) (Fig. 7C). The immunofluorescent staining sections for TNF-α further indicate less of an inflammatory response triggered by 700-EDA/HA-SH/ADSCs hydrogels (Fig. 7A).

Vascular network formation is an essential indicator of diabetic wound healing. Immuno-histochemical staining of CD31 and α-SMA shows that there are obviously more vessels formed at the wounds treated by 700-EDA/HA-SH/ADSCs hydrogels compared to the PBS treated group at day 21 (ESI Fig. S27†). Moreover, at day 21, more mature micro-vessels are augmented in the 700-EDA/HA-SH/ADSCs hydrogel treated group ($p < 0.05$) (Fig. 7D and E). The pro-angiogenic cytokine VEGF expressed in wound sections was also determined and the images of immunohistochemical staining as well as its quantification level are shown as in ESI Fig. S27† and 7F. The secretion of VEGF is significantly promoted by 700-EDA/HA-SH/ADSCs hydrogels. At days 11 and 21, the VEGF level is 1.2-fold ($p < 0.01$) and 0.3-fold higher ($p < 0.05$) than that of the no-treatment group. The presence of co-localized positively stained CD31 and α-SMA cells in immunofluorescent staining sections is strong evidence of vasculature formation and this may explain the accelerated wound healing (Fig. 7B).

Keratin is a major component of keratohyalin granules and is a known factor in wound healing. Here, we generated Keratin-10 (which is secreted in the suprabasal layer) stained sections to analyze the progress of keratinocytes migrating into the wound center. A significantly higher level of re-epithelialization is observed at the wounds treated by the 700-EDA/HA-SH/ADSCs

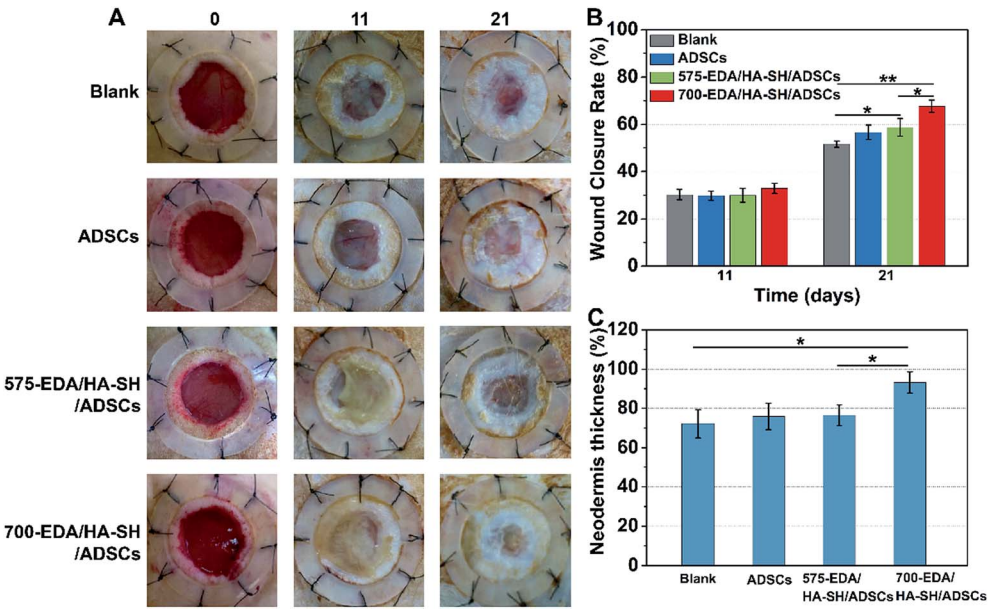


Fig. 6 Wound closure in humanized wound beds in diabetic rats. (A) Representative images of wound closure during 21-day *in vivo* experiments. (B) The quantification of the wound closure rate (%) over a 21-day period. (C) Percentages of newly-formed tissue thickness at 21 days post-wounding. 700-EDA/HA-SH/ADSCs hydrogel treated wounds show significantly promoted healing compared to the PBS group ($n = 8$). *$p < 0.05$; **$p < 0.01$.

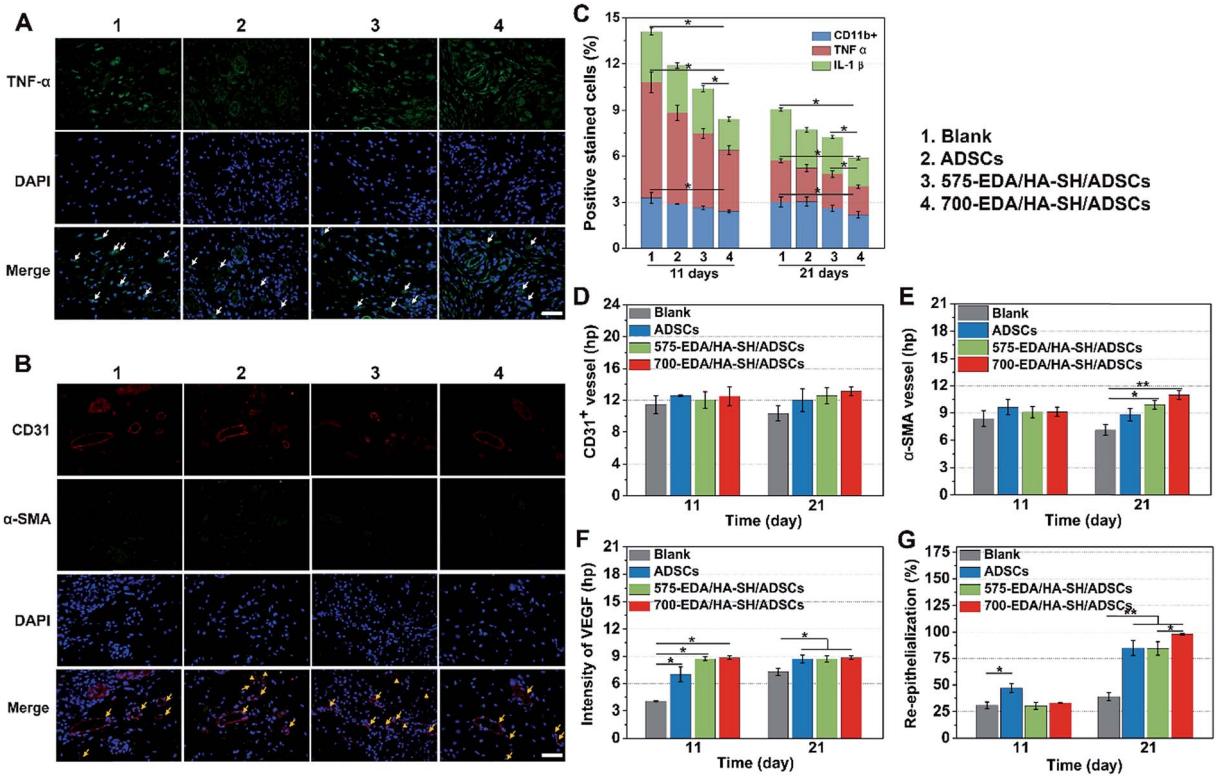


Fig. 7 The wounds treated with injectable 700-EDA/HA-SH/ADSCs hydrogels exhibit fewer inflammatory cells and more newly formed vasculature in diabetic rats. (A) Representative immunofluorescent images of tissue sections at 11 days post-wounding stained for TNF-α (green) and DAPI staining for nuclei (blue). (B) CD31 (for the endothelial marker, red), α-SMA (for the endothelial myofibroblast marker, green), and DAPI (for cell nuclei, blue) stained images (21 days post-wounding). The yellow triangles represent CD31+/α-SMA− vessels, and the yellow arrows represent CD31+/α-SMA+ vessels. Scale bar: 100 μm. (C)–(G) The immuno-histochemical analysis of wound sections in diabetic wound beds. (C) The quantification analysis of the positive stained inflammatory cytokines, which indicates total cellular infiltration into the constructs or wound areas as well as the immune response in the surrounding tissue. Less secretion of inflammatory factors is observed in injectable 700-EDA/HA-SH/ADSCs hydrogel treated wounds. (D) and (E) The quantification analysis of blood vessels based on CD31 and α-SMA positive stained vasculature. The injectable hydrogel treated groups exhibit significantly higher vessel density than the PBS group at 11 and 21 days post-wounding. (F) The intensity of VEGF expression in each experimental group. More secretion of VEGF is seen in 700-EDA/HA-SH/ADSCs hydrogel treated wounds. (G) The quantification analysis of the re-epithelialization rate at days 11 and 21 post-wounding. There is a much faster re-epithelialization rate in the injectable 700-EDA/HA-SH/ADSCs hydrogel groups than in the PBS group ($n = 16$ wounds per treatment group). *$p < 0.05$; **$p < 0.01$.

hydrogel compared to the PBS treated group ($p < 0.01$) at 21 days (Fig. 7G and ESI S28†). All of these results demonstrate that 700-EDA/HA-SH/ADSCs hydrogels can effectively inhibit prolonged inflammation, and promote angiogenesis, migration of keratinocytes and re-epithelialization, ultimately accelerating diabetic wound healing.

## Discussion

The evolution of biomaterials for tissue repair and regeneration has been driven by the need to optimize their chemical and biological properties. The development of both safe and efficient hydrogel systems for stem cell delivery for wound healing has become a great challenge. In comparison with other synthetic polymers, HP-PBAE-based hydrogels are especially suitable for the application of wound healing due to the adjustable degradation profile caused by a wide range of monomer availability. The synthesis of HP-PBAEs has proven to be a long-standing challenge and very few HP-PBAEs have been synthesized, using either special monomer combinations or under harsh reaction conditions. In this study, for the first time, we have demonstrated that HP-PBAEs can be synthesized *via* the versatile "A2 + B4" type Michael addition under mild conditions using low-cost commercially available diamines and PEGDAs. The molecular weight, branching structure, terminal groups, and solubility can be kinetically controlled by varying the feed ratio, monomer combination, and reaction time in a facile manner. The resultant HP-PBAEs also demonstrated good bacteriostatic effects in both *Staphylococcus aureus* and *Escherichia coli* (ESI Fig. S11†) as well as good biocompatibility due to small molecule degradation byproducts (ESI Fig. S9†).

The newly generated HP-PBAEs with a high vinyl ratio and high branching degree addressed the limitations of linear PBAEs used in hydrogel formation, such as high molecular weight, rapid gelation time, and high crosslinking degree. HP-PBAEs show fast gelation time with thiolated hyaluronic acid

*via* a "click" thiol–ene reaction. Using combinatorial integration, these hydrogels possess *in situ* forming profiles and versatile degradation rates, which are important characteristics when considering tissue repair and regeneration applications. All of these advantages lead to superior performance, pointing to the promising application of HP-PBAE-based hydrogels in stem cell delivery. The degradation profile showed that we successfully generated a series of biodegradable hydrogels which can be controlled in a wide range of time periods, both *in vitro* and *in vivo*.

To better mimic the human wound healing process, an excisional humanized wound model was employed to evaluate the effectiveness and safety of the HP-PBAE hydrogels. The humanized wound model was created by Gurtner's laboratory.[24,25] This model could be a good tool for skin wound healing because of its better mimicking and recapitulating of human wound repair mechanisms. It has been reported that activated inflammatory cells and excessive pro-inflammatory cytokines like IL-1β, TNF-α,[27,28] and matrix metalloproteinases[16] could cause severe delay in diabetic wound healing. The termination of the inflammatory response at the right time would reverse impaired wound recovery. The *in vivo* data provide evidence that 700-EDA/HA-SH/ADSCs hydrogels significantly down-regulated the inflammatory factors and terminated the prolonged inflammation phase. HP-PBAE-based hydrogels can be a temporary stem cell niche to maintain the encapsulated ADSCs' viability and secretion profile. Meanwhile, they would degrade at an appropriate rate to match the regeneration of new tissues. The 700-EDA/HA-SH/ADSCs hydrogel can indeed promote the secretion of CD31, α-SMA, and VEGF, suggesting a possible mechanism for increased neovascularization and enhanced wound repair.[29] The closure of gaps within epithelia is crucial to maintain the skin's integrity during the biological processes of wound healing.[30] Chronic wounds show proliferative and non-migratory epidermis because of the hostile wound environment.[31] 700-EDA/HA-SH/ADSCs hydrogel treated wounds show significantly accelerated re-epithelialization and wound closure (Fig. 7E). Correspondingly, collagen deposition, angiogenesis and re-epithelialization are enhanced, ultimately accelerating the diabetic wound repair. In addition, in comparison with direct ADSC injection, the 700-EDA/HA-SH/ADSCs hydrogel system exhibits a more significant acceleration rate indicating the synergistic roles of 700-EDA, HA-SH, and ADSCs in wound healing.

## Conclusions

In this work, we report an "A2 + B4" polymerization approach to develop hyperbranched PBAE macromers, traditionally considered as a typical crosslinking reaction leading to the crosslinked structure (gel). By controlling the polymerization kinetics, the well-designed hyperbranched polymers can be prepared through the "A2 + B4" strategy. This "A2 + B4" polymerization methodology can not only address the limitations of linear PBAEs, but also open a new road to the design and preparation of a variety of new HP-PBAEs compared to the conventional approach. The injectable hydrogels produced from HP-PBAEs and HA-SH exhibit a wide range of degradation rates which can match certain tissue regeneration rates. The injectable hydrogel system can function as a delivery system for ADSCs. The *in vivo* application of ADSC seeded hydrogels in both nondiabetic and diabetic wounds have shown promising results in accelerating the wound healing process, such as promoting diabetic wound environments, inhibiting prolonged inflammation, and promoting vasculogenesis and re-epithelialization.

## Animal experiments

6–8 week old male Sprague Dawley (SD) rats with body weights ranging between 180–240 g were used for ADSC harvest, subcutaneous hydrogel implantation, inducing the diabetic rat model and *in vivo* evaluation. The rats were fed *ad libitum* water and a rodent diet, and housed according to the Animal Experimentation of the Chinese Academy of Medical Sciences and Peking Union Medical College Institute of Biomedical Engineering-approved animal care guidelines. All procedures were approved by the Chinese Academy of Medical Sciences and Peking Union Medical College Institute of Biomedical Engineering.

## Author contribution

W. X. W. came up with the original concepts and led the project. W. W. led in the design and synthesis of the macromers and hydrogels, and the animal experiments. Q. X. designed the research, conducted the majority of the experiments, analyzed the data, and wrote the manuscript. L. R. G. participated in the animal experiments. D. Z. Z., W. G. L., U. G. and L. C. helped with manuscript writing. Y. S. G, S. A., and H. Z participated in the macromer synthesis. Y. X. D helped with the optimization of the animal model. F. G. W. helped to guide the potential clinical use. W. X. W supervised the research.

## Conflicts of interest

There are no conflicts of interest to declare.

## Acknowledgements

We gratefully acknowledge Professor Laifeng Song (Cardiovascular Institute and Fuwai Hospital, Chinese Academy of Medical Sciences and Peking Union Medical College, China) for the guidance of the histology analysis. This work was supported by the Science Foundation Ireland (No 13/IA/1962, 10/IN.1/B2981(T), 15/IFA/3037), Health Research Board of Ireland (HRA-POR-2013-412), University College Dublin and DEBRA Ireland, the National Natural Science Foundation of China (No. 51573129 and No. 51473117), and the National Natural Science Funds for Distinguished Young Scholar (No. 51325305).

## Notes and references

1 D. R. Griffin, W. M. Weaver, P. O. Scumpia, D. Di Carlo and T. Segura, *Nat. Mater.*, 2015, **14**, 737–744.

 

2 J. Alijotas-Reig, M. T. Fernández-Figueras and L. Puig, *Clin. Rev. Allergy Immunol.*, 2013, **45**, 97–108.
3 D. Y. Ko, U. P. Shinde, B. Yeon and B. Jeong, *Prog. Polym. Sci.*, 2013, **38**, 672–701.
4 S. Deshayes and A. M. Kasko, *J. Polym. Sci., Part A: Polym. Chem.*, 2013, **51**, 3531–3566.
5 I. M. Geisler and J. P. Schneider, *Adv. Funct. Mater.*, 2012, **22**, 529–537.
6 J. D. Kretlow, L. Klouda and A. G. Mikos, *Adv. Drug Delivery Rev.*, 2007, **59**, 263–273.
7 J. A. Yang, J. Yeom, B. W. Hwang, A. S. Hoffman and S. K. Hahn, *Prog. Polym. Sci.*, 2014, **39**, 1973–1986.
8 A. J. Boulton, L. Vileikyte, G. Ragnarson-Tennvall and J. Apelqvist, *Lancet*, 2005, **366**, 1719–1724.
9 T. Dinh, F. Tecilazich, A. Kafanas, J. Doupis, C. Gnardellis, E. Leal, A. Tellechea, L. Pradhan, T. E. Lyons, J. M. Giurini and A. Veves, *Diabetes*, 2012, **61**, 2937–2947.
10 D. M. Lynn and R. Langer, *J. Am. Chem. Soc.*, 2000, **122**, 10761–10768.
11 A. Akinc, D. M. Lynn, D. G. Anderson and R. Langer, *J. Am. Chem. Soc.*, 2003, **125**, 5316–5323.
12 D. G. Anderson, A. Akinc, N. Hossain and R. Langer, *Mol. Ther.*, 2005, **11**, 426–434.
13 D. G. Anderson, D. M. Lynn and R. Langer, *Angew. Chem.*, 2003, **115**, 3261–3266.
14 J. J. Green, R. Langer and D. G. Anderson, *Acc. Chem. Res.*, 2008, **41**, 749–759.
15 S. Tang, Q. Yin, J. Su, H. Sun, Q. Meng, Y. Chen, L. Chen, Y. Huang, W. Gu, M. Xu, H. Yu, Z. Zhang and Y. Li, *Biomaterials*, 2015, **48**, 1–15.
16 S. A. Castleberry, B. D. Almquist, W. Li, T. Reis, J. Chow, S. Mayner and P. T. Hammond, *Adv. Mater.*, 2015, 1809–1817.
17 C. Zhang, T. An, D. Wang, G. Wan, M. Zhang, H. Wang, S. Zhang, R. Li, X. Yang and Y. Wang, *J. Controlled Release*, 2016, **226**, 193–204.
18 D. M. Brey, I. Erickson and J. A. Burdick, *J. Biomed. Mater. Res., Part A*, 2008, **85**, 731–741.
19 A. M. Hawkins, M. E. Tolbert, B. Newton, T. A. Milbrandt, D. A. Puleo and J. Z. Hilt, *Polymer*, 2013, **54**, 4422–4426.
20 D. G. Anderson, C. A. Tweedie, N. Hossain, S. M. Navarro, D. M. Brey, K. J. Van Vliet, R. Langer and J. A. Burdick, *Adv. Mater.*, 2006, **18**, 2614–2618.
21 C. Gao and D. Yan, *Prog. Polym. Sci.*, 2004, **29**, 183–275.
22 Y. Zheng, S. Li, Z. Weng and C. Gao, *Chem. Soc. Rev.*, 2015, **44**, 4091–4130.
23 H. R. Kricheldorf, *J. Polym. Sci., Part A: Polym. Chem.*, 2009, **47**, 1971–1987.
24 R. D. Galiano, J. Michaels, V. M. Dobryansky, J. P. Levine and G. C. Gurtner, *Wound Repair and Regeneration*, 2004, **12**, 485–492.
25 V. W. Wong, M. Sorkin, J. P. Glotzbach, M. T. Longaker and G. C. Gurtner, *J. Biomed. Biotechnol.*, 2011, **2011**, 1–8.
26 Y. Lim, S.-M. Kim, Y. Lee, W. Lee, T. Yang, M. Lee, H. Suh and J. Park, *J. Am. Chem. Soc.*, 2001, **123**, 2460–2461.
27 S. K. Beidler, C. D. Douillet, D. F. Berndt, B. A. Keagy, P. B. Rich and W. A. Marston, *J. Cardiovasc. Surg.*, 2009, **49**, 1013–1020.
28 S. Barrientos, O. Stojadinovic, M. S. Golinko, H. Brem and M. Tomic-Canic, *Wound Repair and Regeneration*, 2008, **16**, 585–601.
29 Z. Liu and O. C. Velazquez, *Society for Dermatological Research*, 2010, **52**, 99–105.
30 S. R. K. Vedula, G. Peyret, I. Cheddadi, T. Chen, A. Brugués, H. Hirata, H. Lopez-Menendez, Y. Toyama, L. Neves de Almeida, X. Trepat, C. T. Lim and B. Ladoux, *Nat. Commun.*, 2015, **6**, 6111.
31 S. A. Eming, P. Martin and M. Tomic-canic, *Sci. Transl. Med.*, 2014, **6**, 265sr6.